# ELECTRON CLOUD BUILDUP IN THE ISIS PROTON SYNCHROTRON AND RELATED MACHINES

G Bellodi*, ASTeC Intense Beams Group, RAL, Chilton, Didcot OX11 0QX, UK

*Abstract*

Electron cloud formation and the associated effects of beam loss and instabilities have been observed in high intensity proton machines such as the LANL PSR and the CERN SPS. A program has recently been launched at the Rutherford Appleton Laboratory (UK) to understand the lack of electron cloud induced instabilities in the operations of the 160 kW 70-800 MeV ISIS synchrotron. Simulations have been carried out using a newly developed version of the CERN ECLOUD code [1, 2] to model the main features of the electron cloud build-up in a representative field-free region of the ISIS ring. A comparative study has also been undertaken to gauge electron-proton (e-p) related problems/limitations in possible future proton machines for spallation neutron sources (ESS) or neutrino factories (ISIS MW upgrade).

Table 1: ISIS synchrotron parameters.

| | |
|---|---|
| Repetition rate (Hz) | 50 |
| Injection energy (MeV) | 70 |
| Injection type | $H^-$ multi-turn |
| Injected intensity (ppp) | $2.8 \times 10^{13}$ |
| Extraction energy (MeV) | 800 |
| Extracted intensity (ppp) | $2.5 \times 10^{13}$ |
| Extraction type | single turn |
| Nominal betatron tunes | $Q_h = 4.31$, $Q_v = 3.83$ |
| Efficiencies (inj., trapping, extr.) | $98\%$, $90\%$, $> 99.9\%$ |
| RF frequency sweep (MHz) | 1.3-3.1 |
| Magnet excitation | 50 Hz sinusoidal |
| Peak volts per turn (kV) | 140 |
| Harmonic number | 2 |

## INTRODUCTION

Unlike other high intensity proton machines (such as the LANL PSR and the CERN SPS) that have been affected by electron-cloud induced instabilities, the ISIS proton synchrotron at the Rutherford Appleton Laboratory (UK) has never reported problems that could be traceable to this effect in its more than 20 years of operations. Understanding this singular behaviour is therefore both relevant to a complete picture of the dynamics of electron-proton interactions, and also, on a more practical side, for the planning of future accelerators, should any ISIS features be proven to suppress the effect.

An experimental programme to observe electron-proton instability in ISIS was first attempted around 1995 by G. H. Rees [3]: a coasting beam of $4 \times 10^{13}$ protons was stored at 70 MeV and transverse rms emittances of approximately 50 $\pi\mu$rad-m, but no high-frequency coherent transverse motion was observed in either transverse plane. A more recent programme of observations with the use of gas ionisation beam profile monitors has only just started and has not produced any conclusive results to date.

In this paper we present comparative simulation results for ISIS, the Proton Storage Ring at LANL and ESS [4], a proposal for a future generation European spallation neutron source, obtained with the code ECLOUD [1, 2], originally developed at CERN and here adapted for modelling high intensity long bunch proton machines. The study is limited to the EC buildup and dissipation in a representative field-free or dipole field section of the ring; instability issues have not been addressed so far. A similar study, though restricted to areas of the machines with no external magnetic fields, has been recently undertaken by M. Furman and M. Pivi [5] with the use of their simulation code POSINST [6, 7]. A comparison with our results for the same input parameters shows good agreement.

### *ISIS*

ISIS [8] is presently the world's most powerful pulsed neutron source. Its operational values are summarised in Table 1. Typically $2.8 \times 10^{13}$ protons are accumulated during the $200\mu$s injection process: the beam is effectively unbunched during injection and the $H^-$ ions are stripped with an $Al_2O_3$ foil as they enter the ring acceptance. Acceleration from 70 to 800 MeV takes place over the 10 ms sinusoidal field ramp; trapping of the unbunched beam is concentrated in the first 1 ms and most of the losses ($\sim 10\%$) occur during this process, though they are efficiently intercepted by momentum collimators. The ISIS vacuum chamber is partly made of Stainless Steel (field free sections) and partly ceramic ($97.6\%$ alumina) with StSt RF shields (dipoles and quadrupoles) sitting on MACOR® supports: its walls are smoothly profiled at an approximately constant ratio to the beam radii and present a rectangular cross section.

## SIMULATION MODEL

A detailed description of the simulation code ECLOUD can be found elsewhere [9]. For the purpose of this study the code has been adapted for treatment of non-relativistic superbunches: in particular it has proven essential to use a precise method of resolving the 3D electron kinematics under the accelerating field of the beam and the space charge

* g.bellodi@rl.ac.uk

forces (in our case a $4^{th}$ order Runge-Kutta integration), and to use a very refined slicing inside the bunch (of the order of several thousands of slices), necessary for an accurate tracking of the faster electrons.

Primary electrons are produced either by residual gas ionisation or as a result of lost protons hitting the chamber walls. The ionisation probability per unit length per proton is given by:

$$n_e^i(m^{-1}) = 3.3\sigma_i[\mathrm{Mbarn}] \times p[\mathrm{Torr}] \times \frac{294}{T[\mathrm{K}]}, \quad (1)$$

where $p$ is the gas pressure, $T$ the temperature (assumed 294 K) and $\sigma_i$ is the ionisation cross-section (typically assumed equal to 2 Mbarns).

As a recently added feature, the contribution from proton losses is taken to be:

$$n_e^{pl} = \eta n'_{pl}, \quad (2)$$

where $n'_{pl}$ is the number of lost protons per proton per unit length, and $\eta$ is the electron yield per proton collision. For PSR we assume a beam loss fraction of $\sim 4 \times 10^{-6}$ per revolution. In ISIS most of the losses ($7\%$ of the beam) occur during the first 2 ms of the cycle and in the modelling we simply consider an average loss fraction between revolutions 500 and 1000 ($1.24 \times 10^{-4}$). For ESS we take a limit of $0.01\%$ of lost beam during the first 250 revolutions, which yields a loss factor per revolution of $4\times10^{-7}$. A constant yield efficiency of 100 electrons per proton lost at the wall is then assumed, independent of the proton incident energy and/or collision angle. Electrons produced by proton losses are generated at the walls with a Gaussian energy distribution centered at 10 eV and with $\sigma$ = 5eV, whereas ionisation electrons are generated at rest inside the beam.

These primary electrons are then propagated in the chamber under the influence of external magnetic fields, the beam field, the electrons' space charge force, the beam and the electrons' image fields. When one of these macro-electrons hits the walls, it is either absorbed or re-emitted as a secondary (true secondary, elastically reflected or rediffused) and its initial electric charge is changed according to the value of the secondary emission yield computed for that particular incident energy and angle. In this study we use a fit [10] to secondary emission measurements for Stainless Steel obtained at SLAC for a chemically passivated but not conditioned sample: the fit has been scaled so that the maximum value of the secondary yield is $\delta_{max} = 1.5$ at $E_{max} = 300$ eV. We take into account both the elastic backscattered and the rediffused components. A critical parameter is the secondary yield at very low incident energies ($E_0 < 10$ eV) which influences the survival of electrons at the end of the interbunch gap. Unfortunately this quantity is difficult to determine experimentally and is currently an uncertainty of the model. In this study we adopt the conventional assumption of $\delta(0) \sim 0.4$, and compare it with the case where we assume $\delta(0) \sim 1.0$ following some recent measurements obtained at CERN for a Copper sample [11].

The machine parameters adopted in this study are summarised in Table 2. The ISIS beam energy corresponds to the value at injection, where most of the losses occur. Bunches are modelled with a parabolic longitudinal profile and Gaussian transverse distribution with RMS sizes as per Table 2. The chamber has fixed dimensions and a cylindrical symmetry for PSR, while for ISIS and ESS its cross-section is rectangular and profiled so as to maintain a roughly constant ratio between its radius and the beam radius at any one point in the cycle. A representative section of the machine is selected and the bunch and interbunch gap divided into $N_b$ and $N_g$ slices respectively (roughly corresponding to the same time step). The numbers chosen here (in particular for the bunch slices) are the minimum ones at which convergence in the results was achieved.

## FIELD FREE SIMULATIONS

Saturation of the electron linear density in the machine chamber is reached after the passage of just a few bunches. In all three cases the mechanism of EC buildup is through trailing edge multipacting: during the bunch passage most of the electrons are trapped inside the beam and do not reach the walls for secondary production. It is only when the beam field gets weaker at the tail of the bunch that the electrons can escape and multiply at the walls with a fast rise in their line density; following this, most of them will just dissipate in the interbunch gap and only a fraction survives to be trapped by the next bunch.

Fig. 1 shows the peak value for the EC line density in ISIS to be just under 0.3 nC/m, compared to 1 nC/m for PSR and 3nC/m for ESS. The latter two present a similar pattern of growth, whereas in ISIS, on one hand the higher loss fraction causes some EC formation inside the bunch (due to the primaries), and on the other, the much longer interbunch gap accounts for a more pronounced EC dissipation between bunches. Fig. 2 shows the average flux of electrons (in $\mu$A/cm$^2$) incident upon the chamber walls. One notices that the flux is much larger for PSR and ESS than it is for ISIS (by about a factor of 5). Fig. 3 shows the neutralisation level within the beam, i.e. the ratio between the number of electrons and protons contained within the 1-$\sigma$ ellipse around the bunch centre. Its minimum level at the centre of the bunch is higher for PSR than it is for ISIS or ESS, which could indicate a lower probability for the latter two to be affected by e-p instability.

### *Trailing edge multipacting in rectangular geometry*

The dynamics of trailing edge multipacting presents slightly different features in the three cases considered. In PSR, both the chamber and the beam are (transversely) circular, so the electron cloud buildup (in a field free section of the machine) is isotropic: the electron distribution at the walls is uniform along the circumference and so are the impact energy, angle or secondary emission yield pro-

Table 2: Parameters used for the PSR, ISIS and ESS simulations

| Parameter | ISIS | PSR | ESS |
|---|---|---|---|
| *Machine parameters* | | | |
| Ring circumference (m) | 163.3 | 90 | 220 |
| No. bunches | 2 | 1 | 1 |
| Beam energy (GeV) | 1.014 | 1.735 | 2.272 |
| Bunch population ($10^{13}$) | 1.25 | 5 | 23.4 |
| Bunch length (ns) | 232 | 254 | 560 |
| Interbunch gap (ns) | 470 | 103 | 246 |
| Pipe semi-axes (cm) | (6.3,8) | (5,5) | (5.8,5.2) |
| RMS bunch sizes (cm) | (2.3,3.4) | (1,1) | (1.45,1.3) |
| Residual gas pressure (nTorr) | 500 | 10 | 75 |
| Temperature (K) | 294 | 294 | 294 |
| Proton loss rate ($10^{-9}$p/m) | 763 | 44 | 1.8 |
| | | | |
| *Simulation parameters* | | | |
| Ionisation cross-section (Mbarns) | 2 | 2 | 2 |
| Proton-electron yield | 100 | 100 | 100 |
| Peak SEY | 1.5 | 1.5 | 1.5 |
| Energy at peak SEY | 300 | 300 | 300 |
| SEY at $E_0$=0 | 0.4 | 0.4 | 0.4 |
| $\delta_e(E_{max}) + \delta_r(E_{max})$ | 0.6 | 0.6 | 0.6 |
| Bunch slices ($N_b$) | 500 | 8000 | 8000 |
| Gap slices ($N_g$) | 1000 | 4000 | 4000 |
| No prim. ME per bunch | 500 | 8000 | 8000 |

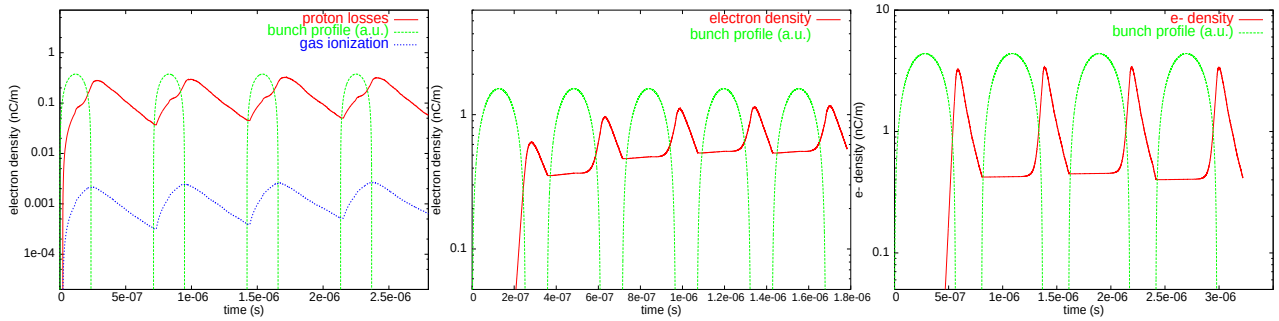


Figure 1: Beam profile (green lines, in a.u.) and electron cloud line density after the passage of a few bunches for ISIS (left, with primary electron generation by either residual gas ionisation - blue line - or proton losses - red line), PSR (centre, proton losses, in red) and ESS (right, proton losses, in red).

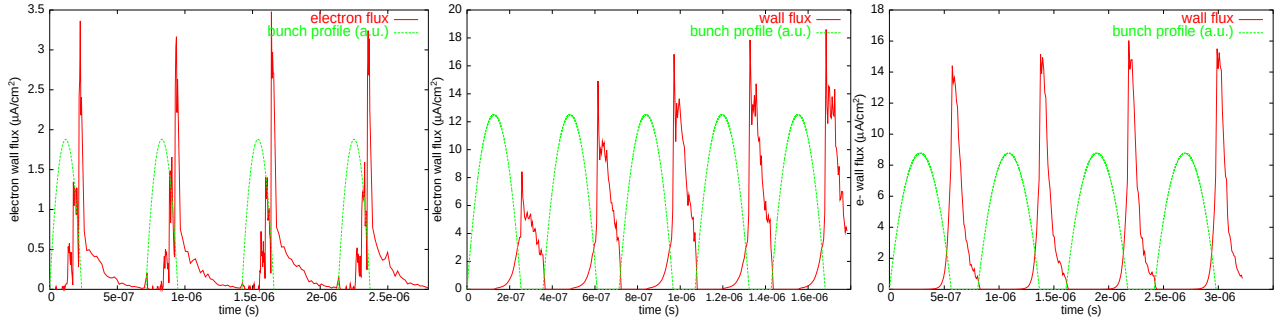


Figure 2: Average electron flux at the chamber wall for ISIS (left), PSR (centre) and ESS (right).

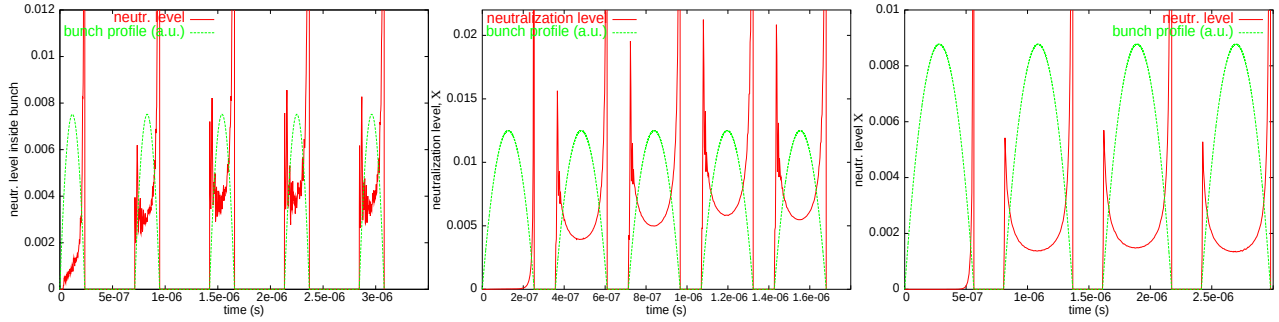


Figure 3: Beam neutralisation factor for ISIS (left), PSR (centre) and ESS (right).

jection (at any one time) along the $x$ or $y$ direction. On the other hand, in ESS and ISIS the beam has an elliptical transverse distribution and the chamber is rectangular. This breaks the isotropy seen for PSR and introduces preferential directions for multipacting, in particular along the two diagonals of the chamber. At the height of electron multiplication in the bunch tail, electrons have nearly head-on collisions along the sides of the chamber, but they impact at a larger angle in the corners and often bounce off the facing wall before being redirected towards the beam (corner trapping). This increases the secondary yield at the corners ($\sim 30\%$ higher than along the sides, see Fig. 5) and 'polarises' the electron multiplication along the diagonals of the chamber. This is particularly evident for ESS, where the multipacting is stronger than in ISIS and the electrons reach higher energies, up to 7 keV (see Fig. 4).

During the interbunch gap this resonance condition is broken as the secondary emission coefficient falls below unity uniformly along the perimeter of the chamber (see Fig. 5) and the electrons assume a more even spatial distribution.

## *Parameter sensitivities*

In this study we have carried out tests to check the sensitivity of the electron cloud buildup to some of the input parameters or physical models adopted in the simulation code.

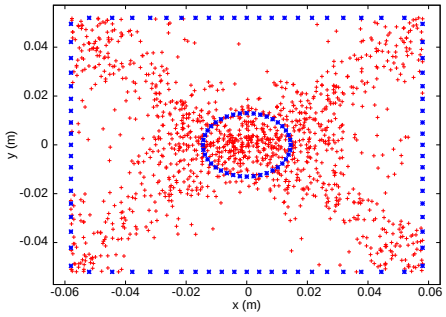


Figure 4: Electron distribution in the ESS rectangular chamber at the height of multipacting in the bunch tail: macroelectrons are shown in red, the boundaries of the bunch and the chamber are in blue.

**Bunch intensity** We have varied the ISIS bunch intensity from its current value ($2.5 \times 10^{13}$ ppp) to the one that might be achieved after completion of the currently ongoing upgrade of the machine to 240 kW, via the installation of a dual harmonic RF system (four extra second harmonic cavities) [12]. The increased longitudinal phase acceptance will make it theoretically possible for up to $3.8 \times 10^{13}$ pro-

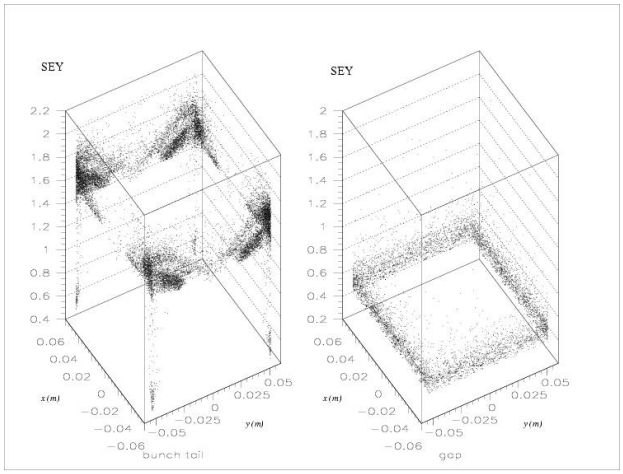


Figure 5: Projection of the SEY coefficient along the perimeter of the chamber at two different time snapshots, in the bunch tail (left) and in the middle of the interbunch gap (right).

tons to be stored in the ring without any additional losses, provided the phase and amplitude of the $h$=4 component are chosen within some tight limits [13]. Assuming the same pattern of losses as in the present machine, the increase in bunch intensity (with all other quantities being kept fixed) brings $\lambda_e$ (EC linear density in the chamber) to double its original peak value (from 0.3 nC/m to 0.6 nC/m).

**Bunch profile** Following some recent studies showing the importance of the bunch longitudinal shape in the dynamics of trailing edge multipacting [14], we have introduced in the simulations the real ISIS bunch profile (averaged over 20 turns of the machine at the start of the cycle shortly after trapping) instead of the parabolic approximation (see Fig. 6).

Just by modifying the shape (in particular adding stronger tails), without changing either the bunch length or its population, the peak $\lambda_e$ increases by nearly $70\%$, showing that the multipacting resonant condition is enhanced.

**SEY model: low-energy and rediffused electrons** Another critical parameter in these simulations is the curve adopted to model the secondary emission yield as a function of the incident energy, and in particular the relative composition of the emitted secondary electrons (i.e. elastically reflected, rediffused and true secondaries) and their energy distribution. The fit used for this study is for StSt data, with $\delta_{max}$=1.5 at $E_{max}$= 300 eV: all three components of the electron spectrum are included, and we assume $\delta_{refl}(E_{max}) + \delta_{red}(E_{max})$=0.6. In the simulation code, secondary electrons are then assigned to one or the other category in proportion to the latter's relative fraction in the overall secondary population at that particular incident energy. If the electron is reflected, its energy is set equal to the incident electron energy minus a small Gaussian smearing; if it is a rediffused its energy is set to E= $E_0 \cdot r^{0.7}$[10] (where

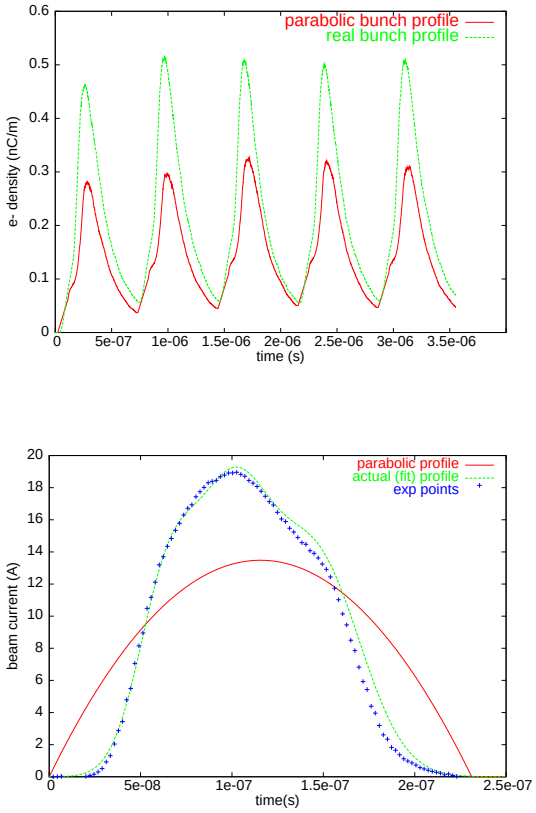


Figure 6: (bottom) ISIS average longitudinal profile as measured at the start of the cycle, superimposed to the parabolic profile; (top) electron-cloud line density buildup for the two different bunch profiles (parabolic in red and as measured in green).

$r$ is a random number uniformly distributed between 0 and 1) and if it is a true secondary its energy is set to conform to a Gaussian distribution centred at 10 eV and with $\sigma$=5 eV.

We have then compared these results to the ones obtained when using a different SEY model (fitting experimental data obtained at CERN on Cu), with the same $E_{max}$ and $\delta_{max}$ values, but with only two secondary electron components included, namely the elastically reflected and the true secondaries (with $\delta_{refl}(E_{max}) + \delta_{red}(E_{max}) \sim 0$). The near absence of any backscattered component at energies higher than 100 eV causes the electron cloud linear density to drop by nearly $40\%$ in its peak value (Fig. 7).

Another important parameter of the SEY model, as mentioned earlier, is the secondary yield at very low incident energy. As this decreases, the ratio between reflected and true secondaries gets larger, until reflection becomes the dominant process for energies below 20 eV. The value of $\delta(0)$ then determines whether these slow electrons are simply absorbed at the walls or backscattered. Assuming $\delta(0) \sim 1$, as some recent experimental observations on Cu seem to suggest [11], we increase the survival time of low-

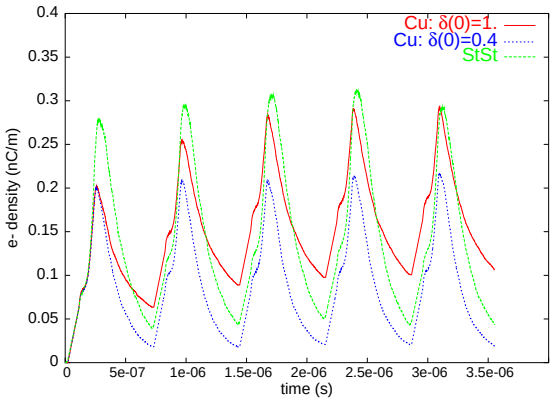


Figure 7: Electron cloud line density for: StSt SEY model (green curve), Cu SEY model with $\delta(0) = 0.4$ (blue curve) and Cu SEY model with $\delta(0) = 1.0$ (red curve).

energy electrons inside the vacuum chambers (due to their high reflectivity), and as a consequence, the peak electron cloud density also increases by nearly $50\%$ (Fig. 7).

The sensitivity of the simulation results to these parameters provides a particularly strong case for further experimental investigations to be carried out in an effort to constrain their values within more accurate and tighter limits.

## DIPOLE FIELD SIMULATIONS

Simulations of electron cloud buildup in dipole fields are currently hampered by difficulties in the physical modelling of the ISIS vacuum chamber. In fact, while the field free sections are entirely metallic and built out of StSt, both dipoles and quadrupoles present a more complex structure. Ceramic vacuum chambers ($97.6\%$ pure $Al_2O_3$) are used in the pulsed magnets of ISIS and radio-frequency shields are interposed between them and the beam to reduce impedances. The fast cycling of the magnets in the synchrotron, however, prohibits the use of solid metal plates because large eddy currents would destroy the quality of the field. The shields are therefore made as grids of stainless steel rods which run parallel to the beam direction and are supported by insulating frames (in MACOR®). In the dipole magnets the vertical sides are solid stainless steel plates, whereas RF screens are inserted above and below the beam (Fig. 8). In the quadrupole magnets RF shields are inserted on all four sides [15]. Part of the difficulties in the electron cloud buildup simulation for such a chamber arise from the fact that it is not yet clear how the presence of the RF screens affects the beam environment and in particular the electron motion. On the other hand, it is also not fully understood how the ceramic chamber behaves under electron/ion bombardment in this particular energy range: only a few experimental datasets on secondary emission are available, which seem to suggest that

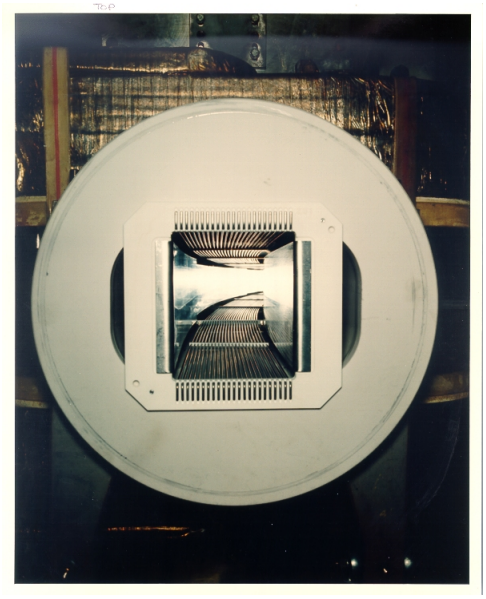

Figure 8: ISIS dipole chamber from the beam's perspective. On the entrance face the rectangular chamber is as wide as the RF shield (22 $\times$ 4.76 = 104.72 mm) and 140 mm high. Dimensions and geometry change within the dipole to follow the beam profile.

the energy dependence of the SEY curve should be similar to that for metal surfaces, but with total yields higher by up to a factor of 5-10. Ceramics, however, would display a time-dependent behaviour due to their electrical charging, eventually approaching a final stationary state characterised by $j(x,t) = 0$ and $\sigma(t) = 1$ (where $j$ is the charge current and $\sigma$ the secondary emission coefficient).

Simulations of EC buildup in the ISIS dipole field at injection ($B = 0.185$ T), in the assumption of a plain stainless steel chamber, show the electron linear density falling to about one third of the value reached in a field-free section of the machine at the same point in the cycle. The electron motion is confined by the magnetic field to the vertical plane and multipacting happen on the horizontal sides of the chamber above and below the beam (see Fig. 9).

A more realistic simulation of the ISIS dipoles is currently dependent on a better understanding of the chamber geometry and on the availability/provision of experimental inputs on secondary emission properties of ceramic surfaces.

## CONCLUSIONS

We have presented preliminary results of EC buildup simulations in the ISIS synchrotron, using a version of the code ECLOUD, adapted for the treatment of intense non-relativistic long bunch proton machines.

For field-free regions we have carried out a comparative study between ISIS, PSR and ESS, assuming the same secondary emission model and specific machine parameters. The following conclusions can be drawn:

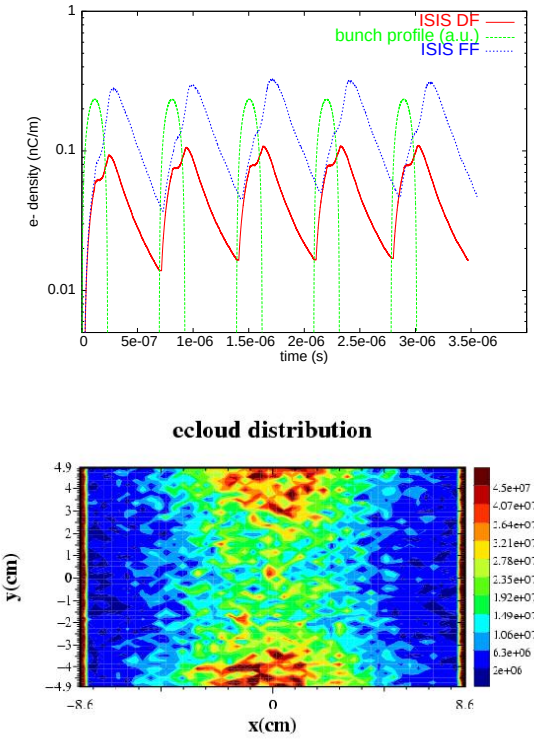


Figure 9: ISIS simulations for a stainless steel dipole chamber: (top) EC buildup (red curve) compared to the field-free case (in blue), and (bottom) electron distribution in the chamber at the beginning of the interbunch gap ($e^-$/cm$^2$).

- when assuming parabolic longitudinal beam distributions, the electron cloud buildup is stronger in PSR and ESS than in ISIS, where the peak electron flux at the wall is smaller by about a factor of 5;
- qualitatively, the pattern of the EC buildup is remarkably similar between PSR and ESS, but different for ISIS, where a) the larger proton loss rate causes some cloud formation even inside the beam (due to the primaries), and b) the larger gap to bunch length ratio (about 4 times that for either ESS or PSR) determines a more pronounced dissipation of the electrons and therefore a weaker buildup.
- The dynamics of trailing edge multipacting has been studied for different chamber geometries (rectangular and circular).
- Sensitivity of the results to the bunch intensity and longitudinal distribution and to the secondary emission model adopted in the simulation code has been assessed. For the latter, in particular, critical parameters have been found to be the elastic electron reflection at low energies and the relative population of the three components of the secondary electron sample (reflected, rediffused and true secondaries) together with their specific energy distributions.
- Simulation results show good agreement with a similar study carried out by M. Furman and M. Pivi [5] using the code POSINST, thus providing proof of benchmarking between the two codes for the cases examined.

A first basic attempt has also been made to simulate EC buildup in dipole regions for ISIS: for a more realistic prediction, however, a clearer understanding of the role played by the RF shields in the vacuum chamber and a precise set of surface measurements on the secondary emission properties of the ceramic walls will be of critical importance.

## ACKNOWLEDGMENTS

The author would like to gratefully acknowledge Giovanni Rumolo and Frank Zimmermann for their collaboration and helpful support in the code development and interpretation of the results. We would also like to thank Daniel Schulte for collaborating in the code update and Miguel Furman, Mauro Pivi and Roberto Cimino for many communications and discussions.

## REFERENCES

[1] F. Zimmermann, *A simulation study of electron-cloud instability and beam induced multipacting in the LHC*, LHC-Project-Report 95 (1997).

[2] F. Zimmermann, *Electron cloud simulations for SPS and LHC*, Chamonix X, CERN-SL-2000-007 (2000).

[3] G. H. Rees, *Aspects of beam stability at ISIS*, Proceedings of the Workshop on Instabilities of High Intensity Hadron Beams in Rings, Upton NY, USA 1999, pp17-21.

[4] *The ESS Project Volume III Update*, at http://www.neutron-eu.net/en/index.php?cat=7 .

[5] M. A. Furman, M. T. F. Pivi, *A preliminary comparative study of the electron-cloud effect for the PSR, ISIS and the ESS*, LBNL-52872/CBP Note 516 (2003).

[6] M. A. Furman, G. R. Lambertson, *The electron-cloud effect in the arcs of the PEP-II positron ring*, LBNL-41123/CBP Note 246 (1997); KEK Proceedings 97-17, p.170 (1997)

[7] M. A. Furman, *The electron cloud effect in the arcs of the LHC*, LBNL-41482/CBP Note 247/CERN LHC Project Report No.180 (1998).

[8] http://www.isis.rl.ac.uk

[9] G. Rumolo and F. Zimmermann, *Electron cloud simulations: buildup and related effects*, Proceedings of the ECLOUD'02 workshop, CERN Yellow Report, CERN-2002-001 (2002).

[10] M. A. Furman and M. T. F. Pivi, *Simulation of secondary electron emission based on a phenomenological probabilistic model*, p.26, LBNL-52807/SLAC-PUB-9912 (2003).

[11] R. Cimino *et al.*, *Can low energy electrons affect high energy physics accelerators?*, Phys. Rev. Lett. **93**, 014801 (2004).

[12] M. R. Harold *et al*., *A possible upgrade for ISIS*, Proceedings of EPAC '98.

[13] C. R. Prior, *Studies of dual harmonic acceleration in ISIS*, ICANS-XII Proceedings, RAL-Report 94-025.

[14] M. T. F. Pivi, M. A. Furman, *Mitigation of the electron-cloud effect in the PSR and SNS storage rings by tailoring the bunch profile*, Proceedings of PAC2003.

[15] Various authors, *Spallation neutron source: description of accelerator and target*, RL-82-006 (1982).